DALTON
FULL PAPER

The chemistry of ruthenium complexes of 1,2-dicyanoethylene dithiolate (mnt^{2-}). Synthesis and characterization of $[Ru^{IV/III}(mnt)_3]^{2-/3-}$ and the derivatives *trans*-$[Ru^{III}(mnt)_2(PPh_3)_2]^-$, *trans*-$[Ru^{III}(mnt)_2(py)_2]^-$ and *trans*-$[Ru^{IV}(mnt)_2(Br)_2]^{2-}$

Rabindranath Maiti, Maoyu Shang and A. Graham Lappin*

University of Notre Dame, Department of Chemistry and Biochemistry, 251 Nieuwland Science Hall, Notre Dame, IN 46556-5670, USA

Received 16th January 2001, Accepted 6th November 2001
First published as an Advance Article on the web 12th December 2001

The chemistry of ruthenium(III) and ruthenium(IV) complexes with 1,2-dicyanoethylene dithiolate(2−) (mnt^{2-}) as ligand has been investigated. The tris-complex $[Ru^{III}(mnt)_3]^{3-}$ is readily prepared and oxidized to $[Ru^{IV}(mnt)_3]^{2-}$. Both complex anions are characterized by X-ray structural analysis. Ligand substitution behavior of the anions has been examined. Reactions of $[Ru^{III}(mnt)_3]^{3-}$ with triphenylphosphine and pyridine are sluggish while reactions of $[Ru^{IV}(mnt)_3]^{2-}$ with these nucleophiles are complex, involving reduction by the displaced mnt^{2-} ligand, to give *trans*-$[Ru^{III}(mnt)_2(PPh_3)_2]^-$ and *trans*-$[Ru^{III}(mnt)_2(py)_2]^-$ respectively. A ruthenium(IV) complex, *trans*-$[Ru^{IV}(mnt)_2(Br)_2]^{2-}$, is formed on treatment of $[Ru^{IV}(mnt)_3]^{2-}$ with Br_2. These three products have also been characterized by X-ray crystallography. In solution, the complexes *trans*-$[Ru^{III}(mnt)_2(PPh_3)_2]^-$ and *trans*-$[Ru^{IV}(mnt)_2(Br)_2]^{2-}$ both lose one axial ligand in rapidly established equilibria. The complex, $[Ru^{IV}(mnt)_3]^{2-}$, undergoes an unusual photochemical rearrangement in the presence of oxygen resulting in formation of $[Ru^{II}(mnts)_2]^{2-}$ where $mnts^{2-}$ is a novel tridentate sulfur-bound ligand.

Introduction

The chemistry of metal ions in unusual coordination environments continues to attract attention. In particular, the ability of reducing ligands coordinated in the stabilization of metals in higher oxidation states provides a fascinating area for study with relevance to both industrial applications and biology.[1] A strategy to prepare such species involves the combination of metal ions which are inert to substitution and ligands which have complex multi-step oxidation mechanisms. In this laboratory, recent work has focused on the chemistry of ruthenuim complexes of dithiolate ligands. There has been extensive study of complexes of ruthenium(II), ruthenium(III) and ruthenium(IV) using 1,1-dithiolate,[2–8] thiolate[5,9–12] and thiaether ligands[13–17] but studies with 1,2-dithiolate ligands are not well represented.[18–21] Over the years, interest in the structural and electronic properties of dithiolate ligands with various metal ions has centered on the non-innocent behavior of the ligands in stabilizing high formal oxidation states.[22–30]

In this paper, the preparation and characterization of ruthenium(III) and ruthenium(IV) complexes of 1,2-dicyanoethylene dithiolate(2−) (mnt^{2-}) are reported. The tris-complex of ruthenium(III), $[Ru^{III}(mnt)_3]^{3-}$ serves as a starting compound which is readily oxidized to $[Ru^{IV}(mnt)_3]^{2-}$. Reactions of $[Ru^{IV}(mnt)_3]^{2-}$ with ligands such as triphenylphosphine, PPh_3, and pyridine, py, lead to the *trans*-axial substituted bis-complexes *trans*-$[Ru^{III}(mnt)_2(PPh_3)_2]^-$ and *trans*-$[Ru^{III}(mnt)_2(py)_2]^-$, formed in a reaction in which the displaced dithiolate acts as a reductant. The ruthenium(IV) complex, *trans*-$[Ru^{IV}(mnt)_2(Br)_2]^{2-}$, is isolated with Br^- as the axial substituent. In both ruthenium(III) and ruthenium(IV) species, there is evidence for axial lability. A preliminary account of part of this work has been published.[31]

Experimental

Materials

The ligand Na_2mnt was synthesized following the reported procedure.[32] Solvents for the electrochemical and spectroscopic work were purified by standard methods.[33] The supporting electrolyte for electrochemical studies, tetra n-butylammonium perchlorate (TBAP), was used as purchased from GFS chemicals. For synthetic experiments commercially available reagent grade solvents (Fisher Scientific) and chemicals (Aldrich) were used as received.

Physical measurements

UV-Visible spectra were run on a Shimadzu UV-3101PC spectrophotometer, and infra-red spectra on a Perkin-Elmer Paragon 1000 FT-IR spectrometer. Electron paramagnetic resonance spectra were obtained with a Varian E-12 X-band spectrometer. Cyclic voltammograms were generated under an argon atmosphere in non-aqueous media with (1–1.5) × 10^{-1} M TBAP as supporting electrolyte and with complex concentrations 1 × 10^{-3} M using a Princeton Applied Research Model 173 potentiostat/galvanostat connected to a Model 175 Universal Programmer. The voltammograms were recorded with a Yokogawa 3025 X–Y recorder. An aqueous Ag/AgCl (with saturated KCl) electrode which contacted the solution through a Vycor tip was used as a reference electrode and a platinum wire as the auxiliary electrode. The working electrode was glassy carbon. All voltammograms were referenced internally to Fc^+/Fc. Spectroelectrochemical experiments were carried out in a short (1 mm) pathlength cell with a platinum minigrid electrode.

 DOI: 10.1039/b100603g

Table 1 Crystal data and structure refinement details

	$[Et_4N]_2[Ru^{IV}(mnt)_2(Br)_2]$	$[Et_4N][Ru^{III}(mnt)_2(PPh_3)_2]$	$[Et_4N][Ru^{III}(mnt)_2(py)_2]$
Formula	$C_{24}H_{40}N_6S_4Br_2Ru$	$C_{52}H_{50}N_5S_4P_2Ru$	$C_{26}H_{30}N_7S_4Ru$
M	801.75	1036.22	669.88
Crystal system	Triclinic	Monoclinic	Monoclinic
Space group	$P\bar{1}$	$P2_1/n$	$C2/c$
a/Å	7.2017(6)	17.188(2)	16.268(5)
b/Å	9.4615(8)	12.8718(11)	14.078(3)
c/Å	12.5828(12)	22.896(3)	15.039(3)
α/°	75.457(7)		
β/°	88.446(7)	101.873(8)	116.82(2)
γ/°	81.798(7)		
V/Å^3	821.38(13)	4957.2(8)	3073.7(13)
Z	1	4	4
μ/mm^{-1}	3.188	0.590	0.810
Reflections: total, observed	2891, 2510	8684, 5936	2709, 2384

X-Ray diffraction data were collected on an Enraf-Nonius CAD4 computer controlled kappa axis diffractometer equipped with a graphite crystal and incident beam monochromator using Mo-Kα radiation (λ = 0.71073 Å) at 293(2) K. All structures were solved by direct methods and full matrix refinement on F^2 was performed with the use of the SHELXTL package.[34] A summary of the crystal data details is given in Table 1. Crystal structures for $[Et_4N]_3[Ru^{III}(mnt)_3]$, $[Ph_4As]_2[Ru^{IV}(mnt)_3]$ and $[Et_4N]_2[Ru^{II}(mnts)_2]$ were reported in an earlier communication.[31]

CCDC reference numbers 174146–174148.

See http://www.rsc.org/suppdata/dt/b1/b100603g/ for crystallographic data in CIF or other electronic format.

Mass spectra were run on a Jeol AX505HA instrument. Magnetic susceptibility measurements were obtained on ground samples in the solid state over the temperature range 200–300 K on a Quantum Design MPMS SQUID susceptometer. Identical measurements at two fields (2 and 20 kG) showed that no ferromagnetic impurities were present.

Syntheses

$[Et_4N]_3[Ru^{III}(mnt)_3]\cdot 2CH_3CN$. Na_2mnt (0.650 g, 3.50 mmol) in water (20 mL) was added with continuous stirring to $RuCl_3\cdot 3H_2O$ (0.207 g, 1.00 mmol) in water (35 mL) under argon. The resulting green solution was warmed at 50 °C for 15 min and the color changed to deep red-brown. To this hot solution, Et_4NBr (0.735 g, 3.50 mmol) was added and the mixture was cooled to room temperature. The crude product was washed with cold water and 2-propanol and recrystallized from CH_3CN–2-propanol (3 : 5). The dark brown crystals were washed with CH_3CN–2-propanol (1 : 3) and dried in air; yield 0.5 g, 50%. The corresponding Ph_4As^+ salt was obtained by the metathesis reaction of $[Et_4N]_3[Ru^{III}(mnt)_3]\cdot 2CH_3CN$ and Ph_4AsCl. Analysis (calculated (found)) for $C_{40}H_{66}N_{11}S_6Ru$: C, 48.31 (47.50); H, 6.68 (6.81); N, 15.49 (15.24); S, 19.34 (18.88)%. IR (KBr pellet, cm^{-1}): ν(CN) 2183(vs), UV-vis (CH_2Cl_2, λ/nm (ε/M^{-1} cm^{-1})): 327 (19050), 405 (14930), 500(sh).

$[Ph_4As]_2[Ru^{IV}(mnt)_3]$. $[Ph_4As]_3[Ru^{III}(mnt)_3]$ (0.167 g, 0.100 mmol) in acetone (10 mL) was treated with I_2 (0.0127 g, 0.050 mmol) in 5 mL CH_2Cl_2 with constant stirring under argon. Immediately the color changed to deep green and the solvent was evaporated slowly to dryness by an argon stream and the dark mass was extracted with 5 mL CH_2Cl_2. The dark green solution was filtered and upon addition of 10 mL petroleum ether (bp 35–60 °C), green microcrystals were obtained. The crystals were filtered, washed with 3 × 2 mL 2-propanol and petroleum ether then evacuated to dryness; yield 0.15 g, 90%. Analysis (calculated (found)) for $C_{60}H_{40}N_6S_6As_2Ru$: C, 55.93 (55.82); H, 3.12 (3.30); N, 6.52 (6.26); S, 14.93 (15.06)%. IR (KBr pellet, cm^{-1}): ν(CN) 2198(vs), UV-vis (CH_2Cl_2, λ/nm (ε/M^{-1} cm^{-1})): 376 (11261), 649 (3429), 681 (3413).

$[Et_4N]_2[Ru^{II}(mnts)_2]\cdot 0.5H_2O$ ($mnts^{2-}$ = $[S_3C_4(CN)_4]^{2-}$). $[Ph_4As]_2[Ru^{IV}(mnt)_3]$ (0.391 g, 0.500 mmol) in acetone (25 mL) was irradiated by Hg-vapor lamp for 6 h. The colour of the solution changed from green to light brown and eventually to brownish red after standing 36 h in air. After solvent evaporation and washing with petroleum ether the product was chromatographed on silica gel using CH_2Cl_2 as eluant and the deep purple band was collected. The solid was collected after precipitation with petroleum ether, and recrystallized from CH_2Cl_2–petroleum ether to produce purple-red crystals; yield 0.087 g, 20%. Analysis (calculated (found)) for $C_{32}H_{41}N_{10}S_6Ru$: C, 44.42 (44.65); H, 4.77 (4.39); N, 16.18 (16.47); S, 22.23 (21.95)%. IR (KBr pellet, cm^{-1}): ν(CN) 2217(m), 2190(vs), UV-vis (CH_2Cl_2, λ/nm (ε/M^{-1} cm^{-1})): 297 (17550), 362 (14676), 400(sh), 524 (9642).

$[Et_4N]_2[Ru^{IV}(mnt)_2(Br)_2]$. $[Et_4N]_2[Ru^{IV}(mnt)_3]$ (0.10 g, 0.13 mmol) in CH_2Cl_2 (10 mL) was purged with argon and treated with 0.3 mL 5% (v/v) bromine in CH_2Cl_2 with constant stirring. The resultant orange-brown solution was diluted with 10 mL methanol, and a brown-black micro-crystalline precipitate was obtained after addition of 15 mL of petroleum ether; yield 0.05 g, 47% (based on the starting compound). Diffraction quality single crystals were grown by layering the reaction mixture with petroleum ether in the presence of bromine vapor. Analysis (calculated (found)) for $C_{24}H_{40}N_6S_4Br_2Ru$: C, 35.95 (35.14); H, 5.02 (4.93); N, 10.48 (10.13); S, 15.99 (15.75)%. IR (KBr pellet, cm^{-1}): ν(CN) 2206(vs), UV-vis (acetone, λ/nm (ε/M^{-1} cm^{-1})): 340 (10301), 560 (1698), 646 (1679), 866 (1207).

$[Et_4N][Ru^{III}(mnt)_2(PPh_3)_2]$. *Method (a).* $[Et_4N]_3[Ru^{III}(mnt)_3]\cdot 2CH_3CN$ (0.10 g, 0.10 mmol) in acetone (10 mL) was treated with PPh_3 (0.08 g, 0.30 mmol) under reflux for 3 h. The solvent was evaporated and after washing with methanol and ether, the crude product was extracted with CH_2Cl_2 (20 mL). Brown microcrystals were obtained after precipitation with petroleum ether; yield 0.026 g, 25%. Analysis (calculated (found)) for $C_{52}H_{50}N_5S_4P_2Ru$: C, 60.27 (60.12); H, 4.86 (4.98); N, 6.75 (6.62); S, 12.37 (12.12); P, 5.97 (6.16)%. IR (KBr pellet, cm^{-1}): ν(CN) 2191(vs), UV-vis (CH_2Cl_2, λ/nm (ε/M^{-1} cm^{-1})): 332 (9970), 421 (9265), 654 (6529).

Method (b). $[Et_4N]_2[Ru^{IV}(mnt)_3]$ (0.10 g, 0.13 mmol) in CH_2Cl_2 (10 mL) was stirred (3 h) with PPh_3 (0.08 g, 0.30 mmol) at room temperature and kept overnight at 10 °C. Brown crystals precipitated and were washed with 3 × 2 mL of methanol to remove an orange impurity; yield 0.73 g, 55%.

Method (c). $[Et_4N]_2[Ru^{IV}(mnt)_2(Br)_2]$ (0.10 g, 0.13 mmol) and PPh_3 (0.08 g, 0.30 mmol) in acetone (10 mL) were stirred with $NaBH_4$ (0.005 g, 0.13 mmol) in methanol (2mL). Brown microcrystals were obtained on slow solvent evaporation and were washed with methanol and ether; yield 0.103 g, 80%.

$[Et_4N][Ru^{III}(mnt)_2(L)_2]$, L = pyridine or imidazole. $[Et_4N]_2[Ru^{IV}(mnt)_2(Br)_2]$ (0.10 g, 0.12 mmol) with either imidazole (0.017 g, 0.25 mmol) or pyridine (0.05 mL, 0.6 mmol) in acetone (10 mL) were stirred for 1 h with $NaBH_4$ (0.005 g, 0.13 mmol) in 2 mL of methanol. Green crystals were precipitated on slow solvent evaporation and were washed with methanol and ether; yield 0.66 g, 85% for imidazole and 0.6 g, 75% for pyridine. Analysis (calculated (found)) for imidazole complex, $C_{22}H_{28}N_9S_4Ru$: C, 40.79 (40.51); H, 4.35 (4.50); N, 19.45 (19.10); S, 19.80 (19.60)%. IR (KBr pellet, cm^{-1}): ν(CN) 2196(vs), UV-vis (acetone, λ/nm (ε/M^{-1} cm^{-1})): 367 (6975), 427 (7190), 453 (9388), 832 (4413). Analysis (calculated (found)) for pyridine complex, $C_{26}H_{30}N_7S_4Ru$: C, 46.62 (45.94); H, 4.51 (4.44); N, 14.63 (14.47); S, 19.14 (18.65)%. IR (KBr pellet, cm^{-1}): ν(CN) 2198(vs), UV-vis (acetone, λ/nm (ε/M^{-1} cm^{-1})): 354 (11124), 406 (9506), 436 (10382), 846 (4186).

Results and discussion

The complex ion, $[Ru^{III}(mnt)_3]^{3-}$, is readily prepared by the reaction of $RuCl_3$ and 3 equivalents of mnt^{2-} in aqueous media under reducing conditions, and has been structurally characterized as the $[Et_4N]_3[Ru^{III}(mnt)_3]\cdot 2CH_3CN$ salt. Cyclic voltammetry studies on this complex, Fig. 1, reveal that there are

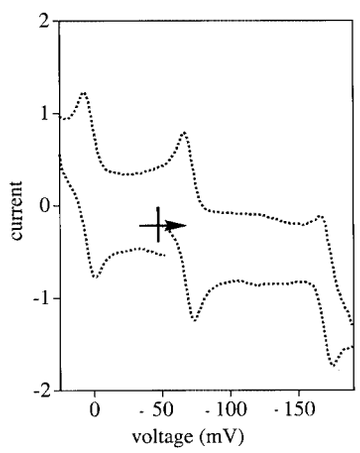

Fig. 1 Cyclic voltammogram of a solution of $[Ru^{III}(mnt)_3]^{3-}$ (1×10^{-3} M in CH_2Cl_2) with 0.1 M TBAP as supporting electrolyte. Scan rate is 100 mV s^{-1}.

two oxidation waves at −0.70 V and +0.03 V and one reduction wave at −1.71 V. The peaks are well-behaved and quasi-reversible with peak–peak separations close to 60 mV. Reduction at −1.71 V leads to a formal ruthenium(II) species with an absorption maximum at 660 nm. This species is very sensitive to aerial oxidation and was not further characterized. However, the direct product of aerial oxidation is the species characterized as $[Ru^{IV}(mnt)_3]^{2-}$ and not $[Ru^{III}(mnt)_3]^{3-}$ which reacts only sluggishly with oxygen under comparable conditions. Consequently, it is concluded that $[Ru^{III}(mnt)_3]^{3-}$ is not an intermediate in the aerial oxidation of $[Ru^{II}(mnt)_3]^{4-}$.

The $[Ru^{III}(mnt)_3]^{3-}$ complex has absorption maxima at 327 nm and 405 nm. Spectroelectrochemical measurements of the oxidation at −0.70 V reveal that the conversion is quantitative and reversible. Absorption bands at 376 nm, 649 nm and 681 nm accompany the formation of the oxidized product which can also be formed by chemical oxidation and is structurally characterized as the $[Ph_4As]_2[Ru^{IV}(mnt)_3]$ salt. The second oxidation wave yields a species with absorption maxima at 412 nm, 503 nm and 635 nm. This species readily decomposes with the formation of disulfide and was not further characterized.

ORTEP drawings of the complex anions $[Ru^{III}(mnt)_3]^{3-}$ and $[Ru^{IV}(mnt)_3]^{2-}$ are presented in Figs. 2 and 3 respectively. The two complexes are six-coordinate with an approximately octahedral distribution of ligand donor atoms around the metal and are quite similar in geometry. In $[Ru^{III}(mnt)_3]^{3-}$ the Ru–S bond averages 2.347 Å which can be compared with 2.376 Å for the tris-1,1-dithiolate, $[Ru^{III}(dtc)_3]$.[4] The twist angle, φ,[35] which most clearly represents distortion from octahedral geometry is 50.2°. The oxidation product, $[Ru^{IV}(mnt)_3]^{2-}$, is significantly more distorted and the average Ru–S distance is 2.343 Å and twist angle $\varphi = 47.1°$. The structure of this species is very similar to that reported for the iron(IV) analogue where φ averages 48.9°.[36,37] Direct comparison with other six-coordinate sulfur bound ruthenium(IV) complexes is not possible. Oxidation of the tris-1,1-dithiolate complex $[Ru^{III}(Et_2dtc)_3]$ produces the dimeric $[Ru_2^{III/III}(Et_2dtc)_5][BF_4]$[6] or seven-coordinated halide ligated compounds $[Ru^{IV}(Et_2dtc)_3Cl]$[7] and $[Ru^{IV}(Me_2dtc)_3I]$[8] with various oxidants, but oxidized species like $[Ru^{IV}(Et_2dtc)_3]^+$ have never been isolated. The average Ru–S distances of these complexes are 2.40 Å for $[Ru^{IV}(Et_2dtc)_3Cl]$ and 2.41 Å for $[Ru^{IV}(Me_2dtc)_3I]$, both significantly longer than the Ru–S distance found in this study.

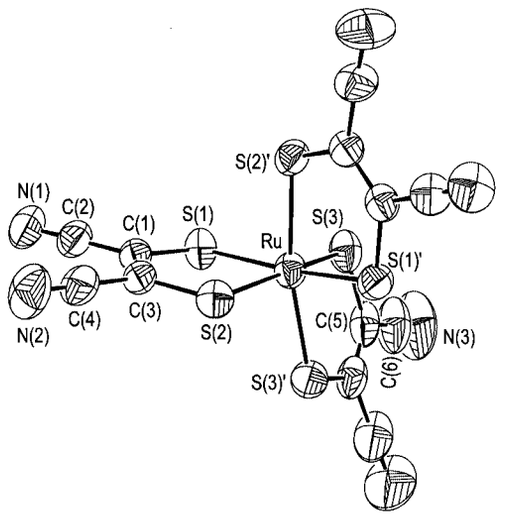

Fig. 2 ORTEP[50] diagram of the anion $[Ru^{III}(mnt)_3]^{3-}$ with 40% thermal probability ellipsoids showing the atomic labeling scheme. Selected bond lengths (Å) and angles (°): Ru–S 2.3468(8), S–C(1) 1.709(4), C(1)–C(1)#2 1.389(7); S–Ru–S#2 87.08(5), S–Ru–S#4 172.18(6).

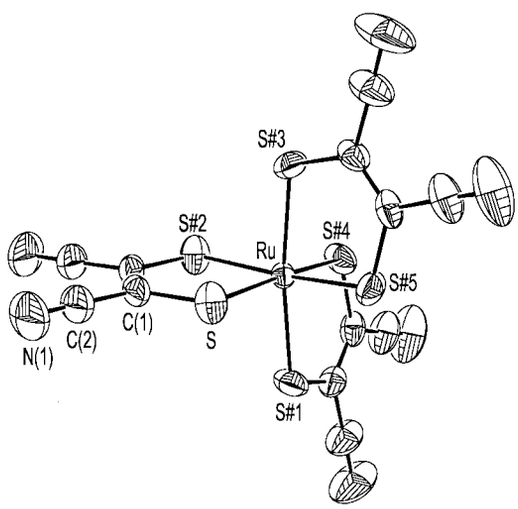

Fig. 3 ORTEP diagram of the anion $[Ru^{IV}(mnt)_3]^{2-}$ with 40% thermal probability ellipsoids showing the atomic labeling scheme. Selected bond lengths (Å) and angles (°): Ru–S(1) 2.3419(13), Ru–S(2) 2.3512(13), Ru–S(3) 2.3349(14), S(1)–C(1) 1.720(5), S(2)–C(3) 1.722(5), S(3)–C(5) 1.725(5), C(1)–C(3) 1.369(6), C(5)–C(5)# 1.349(11); S(1)–Ru–S(2) 86.63(5), S(3)–Ru–S(3)# 86.22(8), S(1)–Ru–S(1)# 169.99(7).

Table 2 EPR data for the ruthenium(III) complexes in frozen CH_2Cl_2 solution at 77 K

Compound	g_1 (A_1)	g_2 (A_2)	g_3 (A_3)
$[Ru^{III}(mnt)_3]^{3-}$	2.114	2.029	1.969
trans-$[Ru^{III}(mnt)_2(PPh_3)_2]^-$	2.055	2.036	1.949
trans-$[Ru^{III}(mnt)_2(py)_2]^-$	2.043 (37.5 G)	2.024 (20.0 G)	1.966 (47.5 G)
trans-$[Ru^{III}(mnt)_2(Im)_2]^-$	2.045 (37.5 G)	2.014 (17.5 G)	1.965 (35.0 G)

Structural studies of higher oxidation state tris-1,2-dithiolate complexes reveal a marked propensity for a trigonal prismatic arrangement of ligand donor atoms.[28–30,38–40] This is ascribed to a combination of significant inter- and intra-ligand S–S interactions on the faces of the complexes and the restricted ligand bite angle.[30,41] In some complexes with metals in higher oxidation states, the mnt^{2-} ligand behaves non-innocently. Two electron oxidation of the ligand is shown in eqn. (1), and is evidenced by a lengthening of the C=C bond and a shortening of the C–S bonds

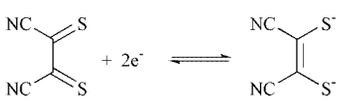

(1)

as a result of the increased π interaction. It is the interaction of these π orbitals that gives rise to the intra-ligand bonding. However, in lower oxidation states, the ligand donor atoms predominantly form the more common, metal directed, octahedral arrangement, maximizing ligand repulsions. It is to this latter group that the compounds described here belong.[18,42] In this instance, the increase in oxidation state is accompanied by a decrease in the C=C bond length in the ligand to 1.362 Å in $[Ru^{IV}(mnt)_3]^{2-}$ from 1.389 Å in $[Ru^{III}(mnt)_3]^{3-}$ and an increase in the S–C bond length to 1.722 Å from 1.709 Å, respectively. This reverse phenomena is also reflected in the infra-red spectra. The CN stretching frequency is at 2183 cm^{-1} for $[Ru^{III}(mnt)_3]^{3-}$ and is shifted to 2198 cm^{-1} for $[Ru^{IV}(mnt)_3]^{2-}$, an unexpected trend as the higher oxidation state presumably contains the more electropositive metal center. There is no evidence in this system that these ligands are behaving non-innocently. The oxidized complex, $[Ru^{IV}(mnt)_3]^{2-}$, is slightly more distorted from octahedral geometry than $[Ru^{III}(mnt)_3]^{3-}$. This appears to be due to a contraction of the ligand bite angle as a result of the shortening of the ligand C=C bond. Restrictions on the ligand bite angle favor distortions towards a trigonal prismatic arrangement but the effect is minimized in these compounds.[30]

The two complexes are paramagnetic. Room temperature magnetic susceptibility measurements yield magnetic moments of 1.59 μ_B for $[Ru^{III}(mnt)_3]^{3-}$ and 2.87 μ_B for $[Ru^{IV}(mnt)_3]^{2-}$. An anisotropic EPR signal can be detected from frozen solutions of $[Ru^{III}(mnt)_3]^{3-}$ at liquid nitrogen temperatures and g_1, g_2 and g_3 values of 2.114, 2.029, 1.969 are calculated, Table 2. There is a previous report of the preparation of $[Ru^{III}(mnt)_3]^{3-}$ and a study of its EPR characteristics.[21] The values of g_1, g_2 and g_3 are in excellent agreement with those obtained in the present study. It was previously concluded from the analysis of the EPR data that the complex should show a significant distortion from octahedral geometry but the present structural analysis reveals that this is not the case. The magnetic susceptibility of $[Ru^{IV}(mnt)_3]^{2-}$ is consistent with two unpaired electrons in a low-spin ruthenium(IV) six-coordinate system. Previously reported ruthenium(IV) 1,1-dithiolate complexes are diamagnetic in nature.[7–9] The $[Ru^{IV}(mnt)_3]^{2-}$ complex does not display an EPR spectrum at liquid nitrogen temperatures and above.

The complex, $[Ru^{IV}(mnt)_3]^{2-}$, undergoes a number of reactions in solution. It can be reduced quantitatively to $[Ru^{III}(mnt)_3]^{3-}$ by an equivalent amount of one electron reducing agents like $NaBH_4$ and PhSH. A slow reaction of $[Ru^{IV}(mnt)_3]^{2-}$ with O_2 takes place on standing in solution in the presence of air. The reaction can be monitored by the formation of a transient room temperature EPR signal with g = 2.029 which is ascribed to a radical formed by oxidation of the ligand backbone. There is also a transformation in the color of the solution from green to brown. Attempts to isolate the brown complex proved unsuccessful. However, FAB/MS results are consistent with an oligomeric species, most likely a dimer. In the presence of light and air, this species undergoes an unusual rearrangement to form a purple product in 25% yield. Isolation of the diamagnetic purple product and characterization reveal that it is $[Ru^{II}(S_3C_4(CN)_4)_2]^{2-}$ where ligand rearrangement has taken place with the addition of one $C_2(CN)_2$ fragment to the parent tris complex for each newly formed ruthenium(II) unit. It is likely that the oxidation of the mnt^{2-} ligand first produces the disulfide form of the ligand[43] and then is transformed into the monosulfide form by elimination of one sulfur, Scheme 1. An ORTEP of the anion is presented in Fig. 4. The ruthenium atom

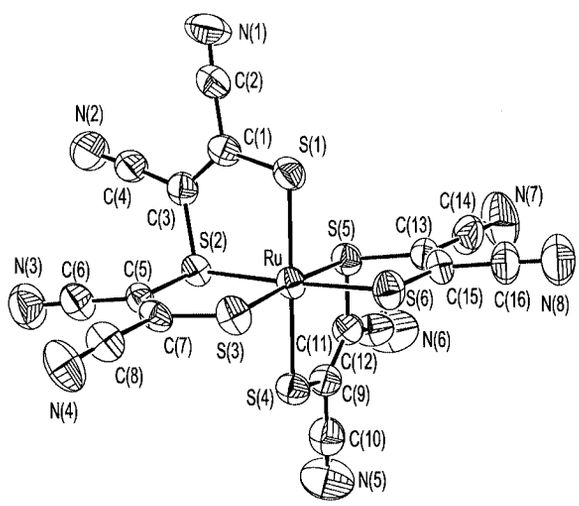

Fig. 4 ORTEP diagram of the anion $[Ru^{II}(mnts)_2]^{2-}$ with 40% thermal probability ellipsoids showing the atomic labeling scheme. Selected bond lengths (Å) and angles (°): Ru–S(1) 2.341(2), Ru–S(2) 2.311(2), Ru–S(3) 2.329(2), Ru–S(4) 2.352(2), Ru–S(5) 2.318(2), Ru–S(6) 2.341(2), S(1)–C(1) 1.690(8), S(2)–C(3) 1.763(7), S(2)–C(5) 1.747(7), S(3)–C(7) 1.710(8); S(1)–Ru–S(4) 176.43(7), S(1)–Ru–S(2) 88.51(7), S(2)–Ru–S(3) 88.08(7), S(2)–Ru–S(5) 93.23(7).

is coordinated by two tridentate sulfur ligands in an octahedral geometry. Average Ru–S bond distances and S–Ru–S *trans* angles are 2.332 Å and 177° respectively. Interestingly, the $[S_3C_4(CN)_4]^{2-}$ ligand appears to favor a facial coordination pattern similar to the tri-thia-macrocycles such as [9]aneS$_3$.[13–15] Indeed the Ru–S distance for the thiaether coordination is very similar for both ligands. In $[Ru^{II}(S_3C_4(CN)_4)_2]^{2-}$, the tricoordinated thiaether sulfur atoms in the two ligands are *cis* to one another. These two sulfur atoms are more strongly bonded to the metal atom compared to the other four as revealed by the shorter Ru–S distances. The S–C bonds related to these sulfur atoms are longer than the others but not much different from those in the tris compounds and clarify that the $mnts^{2-}$ ligand is coordinated in a fashion similar to mnt^{2-}.

The stability of this ruthenium(II) compound, $[Ru^{II}(S_3C_4(CN)_4)_2]^{2-}$, is of interest. Cyclic voltammograms of the $[Ru^{II}(S_3C_4(CN)_4)_2]^{2-}$ compound show a quasi-reversible oxidation wave at +0.42 V, presumably for the $[Ru^{III/II}(S_3C_4(CN)_4)_2]^{-/2-}$ couple, and an irreversible reduction wave at −1.98 V. The related tris complex, $[Ru^{II}(mnt)_3]^{4-}$ has not been isolated by the

reduction of $[Ru^{III}(mnt)_3]^{3-}$ but the reduction potential for $[Ru^{III/II}(mnt)_3]^{3-/4-}$ is −1.71 V. For comparison, the $[Ru^{III/II}([9]aneS_3)_2]^{3+/2+}$ couple is +1.4 V.[13] This range of potentials, over 3 V, is clearly dominated by the change in charge of the complexes in the low dielectric media.

Attempts were made to examine the substitution chemistry of the $[Ru^{III}(mnt)_3]^{3-}$ and $[Ru^{IV}(mnt)_3]^{2-}$ species. Reactions of $[Ru^{IV}(mnt)_3]^{2-}$ with PPh_3, pyridine (py) or imidazole (Im) at ambient temperature lead to reduction at the metal center and formation of ruthenium(III) species, *trans*-$[Ru^{III}(mnt)_2(PPh_3)_2]^-$, *trans*-$[Ru^{III}(mnt)_2(py)_2]^-$ and *trans*-$[Ru^{III}(mnt)_2(Im)_2]^-$ respectively. The displaced mnt^{2-} ligand presumably acts as a reducing agent in these reactions as yields are enhanced with added reductant, $NaBH_4$. These same products may be obtained by direct substitution at $[Ru^{III}(mnt)_3]^{3-}$ but the reaction is slow. When $[Ru^{III}(mnt)_3]^{3-}$ is refluxed with PPh_3, pyridine or with imidazole in acetone the yields of the corresponding substituted compounds are very poor and significant decomposition occurs.

The two complexes, *trans*-$[Ru^{III}(mnt)_2(PPh_3)_2]^-$ and *trans*-$[Ru^{III}(mnt)_2(py)_2]^-$ have been structurally characterized and are shown in Figs. 5 and 6. The ruthenium atom is coordinated pseudo-octahedrally by four sulfur atoms of the ligands and two PPh_3 or py groups are in the *trans* positions. The average Ru–S distance is 2.338 Å for *trans*-$[Ru^{III}(mnt)_2(PPh_3)_2]^-$ and 2.322 Å for *trans*-$[Ru^{III}(mnt)_2(py)_2]^-$. For *trans*-$[Ru^{III}(mnt)_2(PPh_3)_2]^-$, there are two crystallographically independent half molecules in the unit cell. The Ru–S bonds are comparable to those of the reported complex *trans*-$[Ru^{III}(bdt)_2(PMe_3)_2]^-$,[18] but the Ru–P distances, at 2.453 Å, are much longer than the 2.38 Å for PMe_3. It appears that the PPh_3 is more loosely coordinated to the metal center. This may be the result of the less basic nature of the PPh_3 ligands compared with PMe_3. However, there also appears to be a steric interaction between the aromatic rings of PPh_3 and sulfur atoms of the mnt^{2-} ligands shown by the fact that the four sulfur atoms of the ligands are not planar.

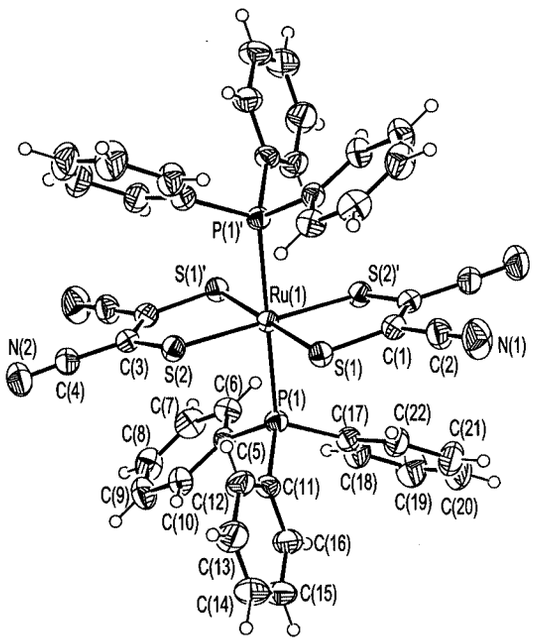

Fig. 5 ORTEP diagram of one of the structures of the anion *trans*-$[Ru^{III}(mnt)_2(PPh_3)_2]^-$ with 40% thermal probability ellipsoids showing the atomic labeling scheme. Selected bond lengths (Å) and angles (°): Ru(1)–S(1) 2.3471(8), Ru(1)–S(2) 2.3327(8), S(1)–C(1) 1.728(3), S(2)–C(3) 1.719(3), C(1)–C(3)# 1.367(4), Ru(1)–P(1) 2.4537(8); S(1)–Ru(1)–P(1) 88.17(3), S(2)–Ru(1)–P(1) 87.75(3). Equivalent values for the second structure (not shown) are: Ru(2)–S(3) 2.3387(8), Ru(2)–S(4) 2.3338(8), S(3)–C(23) 1.729(3), S(4)–C(25) 1.725(3), C(23)–C(25)# 1.365(4), Ru(2)–P(2) 2.4528(8); S(3)–Ru(2)–P(2) 92.31(3), S(4)–Ru(2)–P(2) 91.94(3).

Compounds *trans*-$[Ru^{III}(mnt)_2(py)_2]^-$ and *trans*-$[Ru^{III}(mnt)_2(Im)_2]^-$ are paramagnetic. The magnetic moments of 1.97 and 1.90 μ_B, respectively, correspond to values expected for low-spin d^5 systems. The EPR parameters of these complexes reflect the

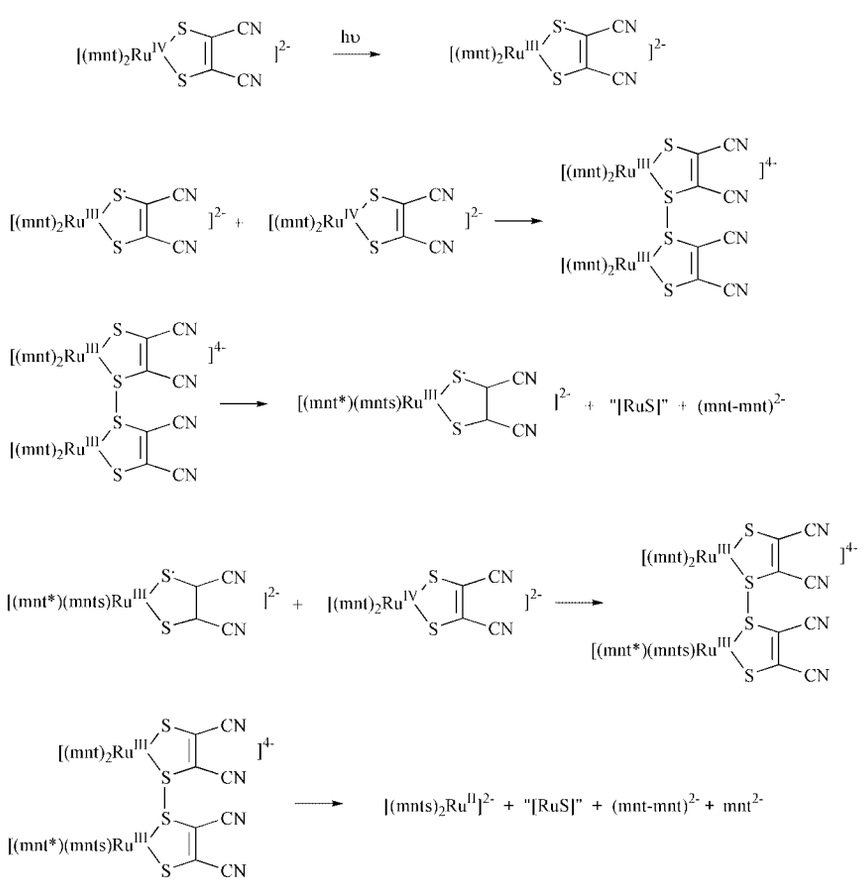

Scheme 1 mnt* is monodentate and $(mnt–mnt)^{2-}$ is the disulfide.

Table 3 Halfwave potentials (V *vs.* Fc^+/Fc) for oxidations and reductions of the ruthenium complexes[a]

Compound	Solvent	Potentials[b] Oxidation couple	Reduction couple
$[Ru^{III}(mnt)_3]^{3-}$	CH_2Cl_2	+0.03 (60), −0.70 (60)	−1.71 (60)
$[Ru^{IV}(mnt)_3]^{2-}$	CH_2Cl_2	+0.03 (60)	−0.70 (60), −1.71 (60)
$[Ru^{II}(mnts)_2]^{2-}$	CH_2Cl_2	+0.42 (70)	−1.98 (E_{pc})
trans-$[Ru^{III}(mnt)_2(PPh_3)]^-$ [c]	CH_3CN	−0.09 (60)	−0.87 (60)
trans-$[Ru^{III}(mnt)_2(PPh_3)_2]^-$ [d]	CH_3CN	−0.12 (60)	−0.96 (60)
trans-$[Ru^{III}(mnt)_2(py)_2]^-$	CH_3CN	0.00 (60)	−1.00 (65)
trans-$[Ru^{III}(mnt)_2(Im)_2]^-$	CH_3CN	−0.17 (60)	−1.30 (60)
trans-$[Ru^{III}(mnt)_2(Br)_2]^-$	CH_2Cl_2	+0.18 (E_{pa}), −0.15 (E_{pc}),	−0.90 (100), −1.48 (60)

[a] Compound concentration is 1×10^{-3} M and electrolyte (TBAP) concentration is (1–1.5) $\times 10^{-1}$ M. Scan rate 100 mV s^{-1}. [b] Half-wave potentials (V *vs.* Fc^+/Fc) correspond to oxidation or reduction of the initial oxidation state of ruthenium. Peak-peak separations (mV) are given in parentheses. E_{pa} and E_{pc} refer to an irreversible couple. [c] In the absence of added PPh_3. [d] In the presence of excess (×150) PPh_3.

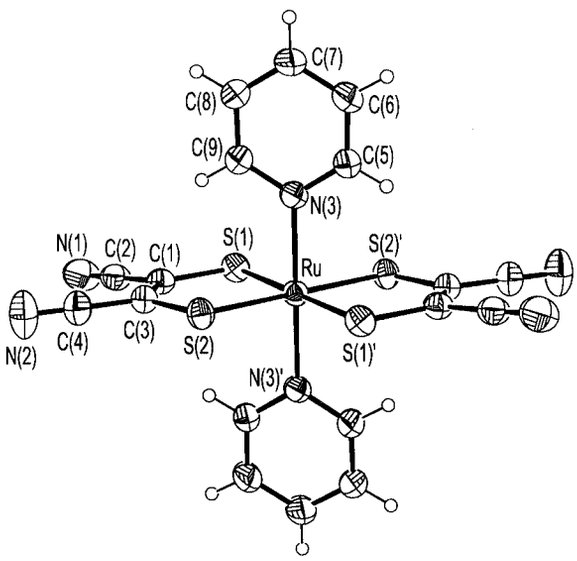

Fig. 6 ORTEP diagram of the anion *trans*-$[Ru^{III}(mnt)_2(py)_2]^-$ with 40% thermal probability ellipsoids showing the atomic labeling scheme. Selected bond lengths (Å) and angles (°): Ru–S(1) 2.3209(10), Ru–S(2) 2.3227(11), S(1)–C(1) 1.732(4), S(2)–C(3) 1.730(4), C(1)–C(3) 1.364(5), Ru–N(3) 2.130(3); S(1)–Ru–N(3) 90.46(8), S(2)–Ru–N(3) 89.61(9).

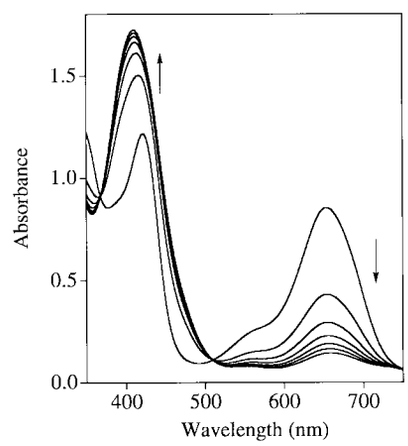

Fig. 7 UV-Vis spectral change of *trans*-$[Ru^{III}(mnt)_2(PPh_3)_2]^-$ (1.3×10^{-4} M) with successive additions of an excess of PPh_3 in CH_2Cl_2 solution. The spectra change in the directions of the arrows with addition of PPh_3. For each successive scan the $[PPh_3]$ is increased by 2.6×10^{-3} M to a maximun of 1.6×10^{-2} M.

solid-state geometry. The solution spectra at 295 K for both *trans*-$[Ru^{III}(mnt)_2(py)_2]^-$ and *trans*-$[Ru^{III}(mnt)_2(Im)_2]^-$ are isotropic with well resolved Ru hyperfine lines centered on $<g>$ values, 2.013 and 2.014, respectively. Spectra of the frozen solution at 77 K are rhombic in nature and the g_{xx}, g_{yy} and g_{zz} values are 2.043, 2.024, 1.966 for *trans*-$[Ru^{III}(mnt)_2(py)_2]^-$ and 2.045, 2.014, 1.965 for *trans*-$[Ru^{III}(mnt)_2(Im)_2]^-$. The ruthenium hyperfine coupling constant values are listed in Table 2.

Cyclic voltammograms of compound *trans*-$[Ru^{III}(mnt)_2(py)_2]^-$ and *trans*-$[Ru^{III}(mnt)_2(Im)_2]^-$ reveal one oxidative and one reductive couple. The voltammograms are reversible and well behaved with peak to peak separations around 60 mV. In *trans*-$[Ru^{III}(mnt)_2(Im)_2]^-$ the oxidation is 170 mV easier and reduction is 300 mV more difficult when compared with *trans*-$[Ru^{III}(mnt)_2(py)_2]^-$ under the same conditions. In view of the π-acceptor properties of imidazole compared with pyridine this is at first surprising but reflects the relative stabilization of the different oxidation states. The potentials are summarized in Table 3.

The solution behavior of the *trans*-$[Ru^{III}(mnt)_2(PPh_3)_2]^-$ complex is of some interest. Dissolution of the yellow crystalline complex in CH_2Cl_2 and in coordinating solvents such as CH_3CN leads to a blue-green solution with an absorption maximum at 654 nm. In the presence of an excess of added PPh_3, an equilibrium with a yellow species is rapidly established. The spectroscopic changes with different amounts of added PPh_3 are shown in Fig. 7. The peak at 654 nm disappears and the behavior suggests an equilibrium of the type shown in eqn. (2). Spectrophotometric titration gives a value of 1.2×10^3 M^{-1} for K_1. The equilibrium is rapidly established with a second-order formation rate constant ≥ 250 M^{-1} s^{-1}.

$$[Ru^{III}(mnt)_2(PPh_3)]^- + PPh_3 \underset{}{\overset{K_1}{\rightleftharpoons}} \textit{trans}\text{-}[Ru^{III}(mnt)_2(PPh_3)_2]^- \quad (2)$$

Equilibria of this type have previously been observed for *trans*-$[Ru^{III}(S_2C_4F_3)_2(PPh_3)_2]^-$ and *trans*-$[Fe^{III}(bdt)_2(PMe_3)_2]^-$ in solution [18,20] but not for *trans*-$[Ru^{III}(bdt)_2(PMe_3)_2]^-$.[18]

The nature of equilibrium is illuminated by EPR analysis of the solutions. At 295 K, the blue-green solution corresponds to *trans*-$[Ru^{III}(mnt)_2(PPh_3)]^-$ and shows an isotropic signal centered on $g = 2.018$ with superhyperfine coupling from a single spin 1/2 phosphorus nucleus with $<A> = 12.5$ G. In the presence of an excess of PPh_3, the signal shifts to $g = 2.015$ and superhyperfine coupling from two equivalent spin 1/2 phosphorus nuclei with $<A> = 12.5$ G is partly resolved, Fig. 8. At 77 K, the frozen solution (acetone–toluene 1 : 1) exhibits a rhombic spectrum with triplet superhyperfine splitting pattern by two equivalent phosphorus atoms even in the absence of added excess PPh_3. Thus, at low temperature the six-coordinate species is stabilized consistent with a negative enthalpy change for the reaction in eqn. (2). The superhyperfine coupling constants and g values are summarized in Table 2. The related low-spin d^5 system $[Fe^{III}(bdt)_2(PMe_3)_2]^-$ shows similar behavior.[42]

Cyclic voltammetry on solutions of *trans*-$[Ru^{III}(mnt)_2(PPh_3)_2]^-$ in Fig. 9 shows two well resolved signals. Oxidation occurs at −0.09 V and reduction to a ruthenium(II) species at −0.87 V. These peaks shift to −0.12 V and −0.96 V respectively

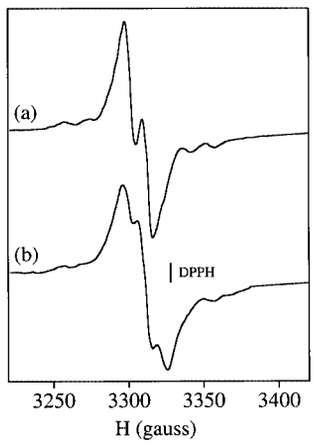

Fig. 8 EPR solution spectra of *trans*-$[Ru^{III}(mnt)_2(PPh_3)_2]^-$ (1×10^{-4} M) in CH_2Cl_2 solution at 295 K: (a) in the absence of added excess PPh_3 (b) in the presence of 1.5×10^{-2} M excess PPh_3. Both signals are located on $g_{av} = 2.018$ with a hyperfine coupling constant from Ru of 22.5 G and a superhyperfine coupling constant from P of 12.5 G.

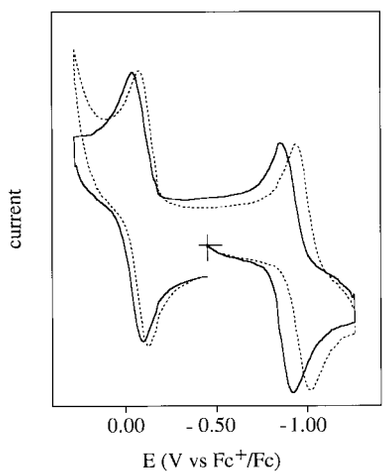

Fig. 9 Cyclic voltammogram of a solution of *trans*-$[Ru^{III}(mnt)_2(PPh_3)_2]^-$ (10^{-3} M) in CH_2Cl_2 with 0.1 M TBAP supporting electrolyte: (——) in the absence of added excess PPh_3 (- - -) in the presence of 1.5×10^{-2} M excess PPh_3. Scan rate 100 mV s^{-1}.

on addition of a 150 fold excess PPh_3 to form the bis-coordinated species. The binding of the second PPh_3 ligand appears to stabilize the higher oxidation state for each redox couple as expected. The potentials are summarized in Table 3.

An attempt was made to oxidize the $[Ru^{IV}(mnt)_3]^{2-}$ species further. A CH_2Cl_2 solution of $[Ru(mnt)_3]^{2-}$ was treated with Br_2 and the isolated product is a diamagnetic dark brown crystalline compound which is structurally determined to be $[Et_4N]_2[Ru^{IV}(mnt)_2Br_2]$. Two bromide groups replace one mnt^{2-} ligand and ruthenium remains in the +4 oxidation state. The compound is six-coordinate with two bromine atoms *trans* to one another. The ORTEP of the anion is shown in Fig. 10. There are many reports of ruthenium(II) and ruthenium(III) compounds coordinated with two halogen and four sulfur donor atoms[44–49] but ruthenium(IV) with this donor set is not known. So the compound *trans*-$[Ru^{IV}(mnt)_2Br_2]^{2-}$ is the first isolated example of this type.

In this complex the average Ru–Br distance, 2.579 Å, is similar to the distances reported for *trans* dibromo compounds such as *cis*-$[Ru^{II}((CH)_4S)(EtS(CH_2)_3SO(CH_2)_3SEt)(Br)_2]$.[47] Thus the bromo groups in *trans*-$[Ru^{IV}(mnt)_2Br_2]^{2-}$ are not more strongly bonded to the ruthenium(IV) center than to the reported ruthenium(II) centers. However, the average Ru–S and S–C distances 2.286 Å and 1.704 Å in *trans*-$[Ru^{IV}(mnt)_2Br_2]^{2-}$ are much shorter than those in the parent compound $[Ru^{IV}(mnt)_3]^{2-}$. The short Ru–S bond distances justify that the

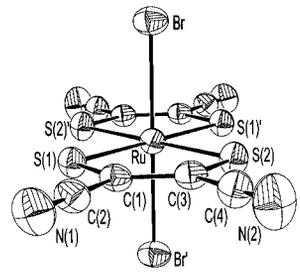

Fig. 10 ORTEP diagram of the anion *trans*-$[Ru^{IV}(mnt)_2(Br)_2]^{2-}$ with 40% thermal probability ellipsoids showing the atomic labeling scheme. Selected bond lengths (Å) and angles (°): Ru–S(1) 2.2840(7), Ru–S(2) 2.2881(7), S(1)–C(1) 1.704(3), S(2)–C(3) 1.704(3), C(1)–C(3) 1.382(4), Ru–Br 2.5790(4); S(1)–Ru–Br 89.48(2), S(2)–Ru–Br 88.73(2).

dithiolate ligands are more strongly bonded to the metal center in *trans*-$[Ru^{IV}(mnt)_2Br_2]^{2-}$ compared to $[Ru^{IV}(mnt)_3]^{2-}$. This may be due to the absence of inter-ligand S–S interactions in *trans*-$[Ru^{IV}(mnt)_2Br_2]^{2-}$ that are present in the tris dithiolate complex.

The solution behavior of *trans*-$[Ru^{IV}(mnt)_2Br_2]^{2-}$ is interesting. The blue dilute acetone solution turns orange in the presence of excess bromide salt. A UV-vis spectral scan with different amounts of added bromide shows the peaks at 560, 646 and 866 nm in the blue solution completely disappear with the generation of new peaks at 483 and 985 nm in the presence of excess added Et_4NBr. Dilution of a solution containing roughly equal proportions of the blue and orange components leads to the spectrum of the initial blue solution. These observations suggest an equilibrium, K_2, involving a bromide ligand which is rapidly established, eqn. (3). Added water in small

$$[Ru^{IV}(mnt)_2Br]^- + Br^- \overset{K_2}{\rightleftharpoons} trans\text{-}[Ru^{IV}(mnt)_2Br_2]^{2-} \quad (3)$$

amounts does not affect the position of the equilibrium but coordination of acetone in the mono-bromo species cannot be ruled out.

The orange solution with excess bromide salt is not EPR active and a cyclic voltammogram of the solution shows two quasi-reversible reduction waves at −0.90 V, −1.48 V and an irreversible oxidation at +0.18 V *vs.* Fc^+/Fc. These do not appear to change significantly with the addition of bromide ion. A spectrophotometric titration gives a value of 1.5×10^3 M^{-1} for the equilibrium constant of the reaction in eqn. (3).

The complex *trans*-$[Ru^{IV}(mnt)_2Br_2]^{2-}$ is reactive towards ligands like PPh_3, pyridine and imidazole, in the presence of $NaBH_4$. The corresponding bis ligated species of Ru(III) of general composition *trans*-$[Ru^{III}(mnt)_2L_2]^-$ (L = PPh_3, Py and Im) are formed.

In conclusion, the ruthenium(IV) complex $[Ru^{IV}(mnt)_3]^{2-}$ provides a useful opening into the synthetic chemistry of both ruthenium(III) and ruthenium(IV) compounds with 1,2-dicyanoethylene dithiolate(2−) as ligand. This contrasts with the sluggish and more complex reactivity of $[Ru^{III}(mnt)_3]^{3-}$. The species *trans*-$[Ru^{III}(mnt)_2L_2]^-$ and *trans*-$[Ru^{IV}(mnt)_2Br_2]^{2-}$ both show significant axial lability which provides further synthetic opportunities.

References

1 E. I. Stiefel, in *Transition Metal Sulfur Chemistry: Biological and Industrial Significance*, ACS Symposium Series No. 653, Washington, DC, 1996, p. 1 and references therein.
2 W.-H. Leung, J. L. C. Chim, H. Hou, T. S. M. Hun, I. D. Williams and W.-T. Wong, *Inorg. Chem.*, 1997, **36**, 4432.
3 D. J Duffy and L. H. Pignolet, *Inorg. Chem.*, 1974, **13**, 2045.
4 L. H. Pignolet, *Inorg. Chem.*, 1974, **13**, 2051.
5 M. Kawano, H. Uemura, T. Watanabe and K. Matsumoto, *J. Am. Chem. Soc.*, 1993, **115**, 2068.
6 B. M. Mattson, J. R. Heiman and L. H. Pignolet, *Inorg. Chem.*, 1976, **15**, 564.

7 K. W. Given, B. M. Mattson and L. H. Pignolet, *Inorg. Chem.*, 1976, **15**, 3152.
8 B. M. Mattson and L. H. Pignolet, *Inorg. Chem.*, 1977, **16**, 488.
9 S. A. Koch and M. Millar, *J. Am. Chem. Soc.*, 1983, **105**, 3362.
10 M. M. Millar, T. O'Sullivan, N. de Vries and S. A. Koch, *J. Am. Chem. Soc.*, 1985, **107**, 3714.
11 S.-L. Soong, J. H. Hain Jr., M. Millar and S. A. Koch, *Organometallics*, 1988, **7**, 556.
12 S. Matsukawa, S. Kuwata and M. Hidai, *Inorg. Chem. Commun.*, 1998, **1**, 368.
13 M. N. Bell, A. J. Blake, H.-J. Küppers, M. Schröder and K. Wieghardt, *Angew. Chem., Int. Ed. Engl.*, 1987, **26**, 250.
14 S. C. Rawle and S. R. Cooper, *J. Chem. Soc., Chem. Commun.*, 1987, 308.
15 S. C. Rawle, T. J. Sewell and S. R. Cooper, *Inorg. Chem.*, 1987, **26**, 3769.
16 T.-F. Lai and C.-K. Poon, *J. Chem. Soc., Dalton Trans.*, 1982, 1465.
17 M. N. Bell, A. J. Blake, A. J. Holder, T. I. Hyde and M. Schröder, *J. Chem. Soc., Dalton Trans.*, 1990, 3841.
18 D. Sellmann, M. Geck, F. Knoch and M. Moll, *Inorg. Chim. Acta*, 1991, **186**, 187.
19 J. Millar and A. L. Balch, *Inorg. Chem.*, 1971, **10**, 1410.
20 L. H. Pignolet, R. A. Lewis and R. H Holm, *J. Am. Chem. Soc.*, 1971, **93**, 360.
21 R. DeSimone, *J. Am. Chem. Soc.*, 1973, **95**, 6238.
22 R. Eisenberg, E. I. Stiefel, R. C. Rosenberg and H. B. Gray, *J. Am. Chem. Soc.*, 1966, **88**, 2874.
23 E. I. Stiefel, R. Eisenberg, R. C. Rosenberg and H. B. Gray, *J. Am. Chem. Soc.*, 1966, **88**, 2956.
24 R. Eisenberg and J. A. Ibers, *J. Am. Chem. Soc.*, 1965, **87**, 3776.
25 R. Eisenberg, *Prog. Inorg. Chem.*, 1970, **12**, 295.
26 M. J. Bennett, M. Cowie, J. L. Martin and J. Takats, *J. Am. Chem. Soc.*, 1973, **95**, 7504.
27 D. Sellmann, A. C. Hennige and F. W. Heinemann, *Eur. J. Chem.*, 1998, 819.
28 M. Cowie and M. J. Bennett, *Inorg. Chem.*, 1976, **15**, 1584.
29 M. Cowie and M. J. Bennett, *Inorg. Chem.*, 1976, **15**, 1589.
30 M. Cowie and M. J. Bennett, *Inorg. Chem.*, 1976, **15**, 1595.
31 R. Maiti, M. Shang and A. G. Lappin, *Chem. Commun.*, 1999, 2349.
32 E. I. Stiefel, L. E. Bennett, Z. Dori, T. H. Crawford, C. Simo and H. B. Gray, *Inorg. Chem.*, 1970, **9**, 281.
33 D. D. Perrin and W. L. F. Armarego, *Purification of Laboratory Chemicals*, 3rd edn., Butterworth-Heinemann, Oxford, 1988.
34 SHELXTL, Version 5, Siemens Industrial Automation, Inc., Madison, WI, 1994.
35 The twist angle, φ, is defined as the angle between the trigonal faces of sulfur donors. It will be 0° for an ideal trigonal prism and 60° for an ideal octahedron.
36 A. Sequeira and I. Bernal, *J. Cryst. Mol. Struct.*, 1973, **3**, 157.
37 G. R. Lewis and I. Dance, *J. Chem. Soc., Dalton Trans.*, 2000, 3176.
38 F. W. B. Einstein and R. D. G. Jones, *J. Chem. Soc. (A)*, 1971, 2762.
39 G. F. Brown and E. I. Stiefel, *Inorg. Chem.*, 1973, **12**, 2140.
40 E. I. Stiefel, Z. Dori and H. B. Gray, *J. Am. Chem. Soc.*, 1967, **89**, 3353.
41 E. I. Stiefel and G. F. Brown, *Inorg. Chem.*, 1972, **11**, 434.
42 D. Sellmann, M. Geck, F. Knoch, G. Ritter and J. Dengler, *J. Am. Chem. Soc.*, 1991, **113**, 3819.
43 H. E. Simmons, R. D. Vest, D. C. Blomstrom, J. R. Roland and T. L. Cairns, *J. Am. Chem. Soc.*, 1962, **84**, 4746.
44 J. Chatt, G. J. Leigh and A. P. Storace, *J. Chem. Soc. (A)*, 1971, 1380.
45 I. P. Evans, A. Spencer and G. Wilkinson, *J. Chem. Soc., Dalton Trans.*, 1973, 204.
46 J. D. Oliver and D. P. Riley, *Inorg. Chem.*, 1984, **23**, 156.
47 D. P. Riley and J. D. Oliver, *Inorg. Chem.*, 1986, **25**, 1825.
48 E. Alessio, G. Mestroni, G. Nardin, W. M. Attia, M. Calligaris, G. Sava and S. Zortel, *Inorg. Chem.*, 1988, **27**, 4099.
49 D. T. T. Yapp, J. Jaswal, S. J. Rettig and B. R. James, *Inorg. Chim. Acta*, 1990, **177**, 199.
50 M. N. Burnett and C. K. Johnson, ORTEP-III, Report ORNL-6895, Oak Ridge National Laboratory, Oak Ridge, TN, 1996.